Supporting Information

Lanthanide nanocomposite with cross-relaxation enhanced near-infrared emissions as ratiometric nanothermometer

Qian Hu[a], Na Kong[a], Yingjie Chai[b], Zhenyu Xing[a], Yukai Wu[a], Jieying Zhang[a], Fuyou Li*[b] and Xingjun Zhu*[a]

[a]School of Physical Science and Technology, ShanghaiTech University, 393 Huaxia Road, Shanghai, 201210, P.R. China.

[b]Department of Chemistry & State Key Laboratory of Molecular Engineering of Polymers & Collaborative Innovation Center of Chemistry for Energy Materials, Fudan University, 2005 Songhu Road, Shanghai 200438, P.R. China.

*Corresponding Authors

E-mail: zhuxj1@shanghaitech.edu.cn; E-mail: fyli@fudan.edu.cn

Materials

Lanthanide oxides including Gd_2O_3 (99.999 %), Yb_2O_3 (99.999 %), Y_2O_3 (99.999 %), Nd_2O_3 (99.999 %), Tm_2O_3 (99.999 %) and cyclohexane (99.9 %) were purchased from Adamas-beta Co., Ltd. Ln_2O_3 (Ln = Gd, Y, Yb, Nd and Tm) were dissolved in a proper amount of hydrochloric acid and re-crystallized to obtain the lanthandie chloride ($LnCl_3$). Oleic acid (OA, 90 %) and 1-octadecene (ODE, 90 %) were purchased from Sigma Aldrich. NaOH (AR) and Gelatins (CP) were purchased from Sinopharm Chemical Reagent Co., Ltd. NH_4F (AR, ≥ 98 %), ethanol (GR, ≥ 99.8 %), and N, N-dimethylformamide (≥ 99.5 %) were purchased from General-reagent. DSPE-PEG (2000 Da) was purchased from J&K Co., Ltd. Tris-buffered saline was purchased from Beyotime Co., Ltd. Hemoglobin was purchased from Aladdin. Intralipid was purchased from Weifang Chensong Intelligent Technology Co., Ltd. Carrageenan was purchased from Mackling Co., Ltd. All chemicals were used as received without further purification.

Characterizations

A Bruker D2 Phaser desktop XRD was used to collect the X-ray diffraction (XRD) data of the as-prepared samples. Transmission electron microscopy (TEM) images were carried out on JEM-1400 Plus emission transmission electron microscope operated at an acceleration voltage of 120 kV.

High-resolution TEM measurements were carried out using 2100 Plus transmission electron microscope operated at an acceleration voltage of 200 kV. HAADF-STEM and elemental mapping images were tested by a JEM-F200 transmission electron microscope. The upconversion and near infrared emission spectra were obtained by using FX2000 and NIR1700 spectrometer (Ideaoptics) irradiated by 808 nm diode laser, respectively. Lifetime Fluorescence Spectrometer (FLS1000, Edinburgh, England) was used to provide the decay curves. All spectra were recorded under identical experimental conditions unless otherwise noted.

Methods

Synthesis of $NaGdF_4$:49%Yb,1%Tm core nanoparticles (CNP)

Typically, 1 mmol lanthanide chloride (0.5 mmol $GdCl_3$, 0.49 mmol $YbCl_3$ and 0.01 mmol $TmCl_3$) were mixed with 10 ml oleic acid (OA) and 10 ml 1-octadecene in a 100-ml three-necked flask. The mixture was then heated to 120 °C and kept for 1 h to obtain a transparent solution. NH_4F (3.4 mmol) and NaOH (2.5 mmol) dissolved in 11 ml methanol was added into the solution when the system is cooled down to 50 °C. After degassing for 30 min at 90 °C to remove methanol, the mixture was heated to 300 °C as soon as possible. Subsequently, the resulting solution was kept at 300 °C for 1.5 h under argon atmosphere. When the mixture was cooled down to room temperature, the nanoparticles were obtained by centrifugation at 12500 rpm for 15 min, and then washed with ethanol and cyclohexane (1:1) solution three times. The core nanoparticles were dispersed in octadecene (ODE) (3 mL) prior to being used for shell coating.

Synthesis of $NaGdF_4$:49%Yb,1%Tm@$NaYF_4$:20%Yb (CS1NP)

The previously synthesized $NaGdF_4$: 49%Yb,1%Tm core nanoparticles were used as seeds for shell coating. One millimole of lanthanide chloride (0.8 mmol YCl_3, 0.2 mmol $YbCl_3$) was added into a mixed solution of 10 mL oleic acid (OA) and 7 mL octadecene (ODE). The mixture was degassed at 60 °C and then heated to 120 °C for 1 h to obtain a transparent solution. Then methanol solution dissolving NH_4F (3.4 mmol) and NaOH (2.5 mmol) was added and the mixture was degassed at 90 °C for 30 min to remove methanol. Immediately afterwards, the reaction was heated to 300 °C under argon atmosphere for 1.5 h before cooling down to room temperature. The CS1NPs were collected under the centrifugation at 12500 rpm for 15 min with the addition of ethanol and cyclohexane (1:1) solution. Nanoparticles were washed for three times before dispersing in ODE (3 ml) for further

use.

Synthesis of $NaGdF_4$:49%Yb,1%Tm@$NaYF_4$:20%Yb@$NaGdF_4$:10%Yb,25%Nd (CS2NP)

CS2NPs were prepared by epitaxial growth on CS1NPs via a solvothermal method similar to CS1NPs synthesis processes. One millimole of lanthanide chloride (0.65 mmol $GdCl_3$, 0.1 mmol $YbCl_3$ and 0.25 mmol $NdCl_3$), 10 ml OA and 7 ml ODE were mixed together in a 100-ml three-necked flask. The precursor solution of the CS2NPs were prepared via the same procedure as mentioned above.

Synthesis of $NaGdF_4$:49%Yb,1%Tm@$NaYF_4$:20%Yb@$NaGdF_4$:10%Yb, 25%Nd@$NaGdF_4$ (DRLNT)

The synthetic procedures for core-multishell nanoparticles were almost the same as CSxNP (x = 1, 2, 3) except for the addition of 1 mmol $GdCl_3$. And the final nanoparticles were dispersed in cyclohexane (10 ml).

Synthesis of $NaYF_4$:49%Yb,1%Tm@$NaYF_4$:20%Yb@$NaYF_4$:10%Yb, 25%Nd@$NaYF_4$ (Y-CS3NP)

The synthetic procedures of $NaYF_4$:49%Yb,1%Tm@$NaYF_4$:20%Yb@$NaYF_4$:10%Yb, 25%Nd@$NaYF_4$ were similar to DRLNT except the use of YCl_3 only for establishing the matrix instead of $GdCl_3$.

Surface modification of DRLNT with 1, 2-distearoyl-sn-glycero-3-phosphoethanolamine-poly(ethylene glycol) (DSPE-PEG)

DSPE-PEG (10 mg) and DRLNT (10 mg) were dispersed in 5 ml dichloromethane and sonicated for 5 min. Then the dichloromethane in the mixture was removed using rotary evaporator. The precipitate was redispersed in 2 ml deionized water and washed by centrifugation (8000 rpm, 5 min) for 2 times to prepare DSPE-PEG modified DRLNT (DRLNT@PEG).

NIR luminescence spectroscopy of nanocomposites

Nanoparticles (CNP, CS1NP, CS2NP, DRLNT and Y-CS3NP) were dispersed in deionized water and the concentrations of Tm^{3+} ions were kept the same in all of the nanocomposite dispersions. For the measurement of NIR luminescence, nanoparticles dispersions were put in a quartz cuvette and NIR emission spectra were collected by an optical fiber spectrometer (NIR1700, Ideaoptics, China) under the excitation of a continuous wave (CW) 808 nm laser at 0.3 W/cm^2.

Measurement of absolute quantum yields

DRLNT and Y-CS3NP powder samples were contained in a quartz sample cell and put in the middle of a barium sulfate coated integrating sphere and then the integrating sphere was mounted on the fluorescence spectrometer (FLS1000, Edinburgh). The excitation and emission ports of the integrating sphere were in 90° geometry from each other in the plane of the spectrometer. An 808 nm fiber coupled laser was used as excitation source. All the spectra collected were corrected with the spectral response of both the spectrometer and the integrating sphere. The response of the detection units including sphere, detectors and monochromators in photon flux was obtained by a calibrated tungsten lamp. The emission quantum yield (QY%) is defined as,

$$\mathrm{QY\%} = \frac{Photons\ emitted}{Photons\ absorbed} \times 100\% = \frac{L_{sample}}{E_{reference} - E_{sample}} \times 100\%$$

where QY% is the quantum yield, L_{sample} is the luminescence intensity, $E_{reference}$ and E_{sample} are the intensities of the excitation source not absorbed by the sample and the reference sample, respectively.

Determination of temperature calibration of DRLNT in aqueous solution

DRLNT@PEG aqueous dispersion (1 ml, 10 mg ml^{-1}) in a quartz cuvette was put in the temperature-adjustable cuvette holder. The change of luminescence intensity with temperature from 10 to 90 °C was measured by an optical fiber spectrometer. Then the NIR emission intensity from 1200 to 1600 nm was collected under the excitation of a continuous wave (CW) 808 nm laser. The emission spectra were measured three times at each temperature point. The ratio of emissions at 1470, 1330 and 1215 nm at each temperature point was given to determine the calibration curve.

Temperature dependence of ion-ion energy transfer and multiphonon relaxation (MPR) rates.

The multiphonon relaxation possibility ($W_p(T)$) between two energy levels connected with temperature can be expressed as follows[1-2]:

$$W_p(T) = W_0 e^{-\alpha \Delta E} \left[\frac{exp(\hbar\omega/kT)}{\exp\left(\frac{\hbar\omega}{kT}\right) - 1}\right]^p \quad (1)$$

where W_0 is the spontaneous transition rate, which is a constant dependent on the phonon density of the matrix, and $\alpha = -ln\varepsilon/\hbar\omega_p$ where ε accounts for the exact nature of the ion-phonon coupling, $\hbar\omega$ represents for phonon energy. Based on the reported works[3-4], in $NaGdF_4$ host, $W_0 = 1 \times 10^8$ s^{-1}, $\alpha = 5 \times 10^5$ cm, and in $NaYF_4$ host, $W_0 = 1 \times 10^7$ s^{-1}, $\alpha = 4.5 \times 10^5$ cm.

When the excitation energy is higher or lower than its absorption energy, known as anti-Stokes or Stokes excitation, the energy difference is provided via p phonons from lattice. The relative temperature behavior of anti-Stokes and Stokes excitation in $NaGdF_4$ and $NaYF_4$ can be given by[1,5]:

$$W_{anti-Stokes}(T) = W_{anti-Stokes}(0)\left[\exp\left(\frac{\hbar\omega}{kT}\right) - 1\right]^{-p} \quad (2)$$

$$W_{Stokes}(T) = W_{Stokes}(0)\{[\exp\left(\frac{\hbar\omega}{kT}\right) - 1]^{-1} + 1\}^{p} \quad (3)$$

Where $W_{anti-Stokes}(0)$ and $W_{Stokes}(0)$ represent for the excitation rates at T = 0 K, respectively. The rates of the multiphonon relaxation in the $^4F_{5/2}\rightarrow{}^4F_{3/2}$ (Nd) (ΔE=1100 cm^{-1}, p=3, $\hbar\omega$=367 cm^{-1}), $^4I_{13/2}\rightarrow{}^4I_{11/2}$ (Nd) (ΔE=2100 cm^{-1}, p=6, $\hbar\omega$=350 cm^{-1}), $^1D_2\rightarrow{}^1G_4$ (Tm) (ΔE=6600 cm^{-1}, p=19, $\hbar\omega$=347 cm^{-1}), $^1G_4\rightarrow{}^3F_{2,3}$ (Tm) (ΔE=6200 cm^{-1}, p=18, $\hbar\omega$=344 cm^{-1}) and $^3H_5\rightarrow{}^3F_4$ (Tm) (ΔE=2400 cm^{-1}, p=7, $\hbar\omega$=344 cm^{-1}) transitions; the anti-Stokes excitation involving the $^2F_{5/2}$ (Yb) and $^4F_{3/2}$ (Nd) levels (ΔE=1500 cm^{-1}, p=4, $\hbar\omega$=375 cm^{-1}), $^2F_{5/2}$ (Yb) and $^3H_4$ (Tm) levels (ΔE=2900 cm^{-1}, p=8, $\hbar\omega$=362 cm^{-1}), cross relaxation processes of ($^1D_2$, $^3H_6$)→($^3F_{2,3}$, $^3F_{2,3}$) (ΔE=1400 cm^{-1}, p=4, $\hbar\omega$=350 cm^{-1}) and ($^6P_{7/2}$, $^3F_3$)→(^6D_J, $^3H_5$) (ΔE=1950 cm^{-1}, p=6, $\hbar\omega$=325 cm^{-1}); the Stokes excitation in the cross relaxation processes ($^1G_4$, $^3H_6$)→($^3H_4$, $^3H_5$) (ΔE=200 cm^{-1}, p=1, $\hbar\omega$=200 cm^{-1}), ($^6P_{7/2}$, $^1G_4$)→(^6D_J, $^3H_4$) (ΔE=350 cm^{-1}, p=1, $\hbar\omega$=350 cm^{-1}) are calculated and presented in Figure S12 to S15.

Calculation of thermometric parameters of DRLNT

Thermal relative sensitivity (S_r):

Thermal relative sensitivity (S_r) of DRLNT is calculated by[6]:

$$S_r = \frac{1}{R}\frac{dR}{dT}$$

where R is the intensity ratio value and T is the temperature.

Repeatability:

The repeatability (Rp) of DRLNT can be defined as[7]:

$$R_p = 1 - \frac{max(|R_c - R_i|)}{R_c}$$

where R_c and R_i stand for the mean value of the thermometric parameter and the measured value each time, respectively.

Uncertainty:

The uncertainty (δT) of DRLNT can be estimated from the errors in the measurement of the ratios, which is defined as[6]:

$$\delta T = \frac{1}{S_r}\frac{\delta R}{R}$$

where δR/R depends on the signal-to-noise ratio of the acquisition setup.

Cytotoxicity of DRLNT.

In vitro cytotoxicity of DRLNT@PEG was measured by methyl thiazolyl tetrazolium (MTT) assays on HEK 293T cells. The cells were planted into a 96-well cell culture plate at 1×10^4 per well and were cultured at 37 °C and 5 % CO_2 for 24 h. After that, different concentrations of DRLNT (0, 50, 100, 150, 200, 300 and 400 μg ml^{-1}, diluted in Dulbecco's Modified Eagle Medium, DMEM) were used in the wells and incubated for 48 h under 37 °C and 5 % CO_2. Then MTT (20 μl; 5 mg ml^{-1}) was added to each well and the assay plate was incubated for another 4 h at 37 °C and 5% CO_2. The optical density OD 490 value (Abs.) of each well was measured three times by a microplate reader (Cytation5, Biotek, America). Cell viability (%) was calculated by the ratio of the treatment group to control group.

Preparation of tissue phantom[8]

The mixture of Tris buffered saline (8 ml) and a certain amount of gelatin (10 w/v%) was heated to 60 °C with constant stirring until the gelatin is completely dissolved. Then hemoglobin (50 μM) and intralipid (0.1 v/v%) were added into the system after the gelatin solution was cooled to room temperature. When the system became a uniform solution, DRLNT@PEG were added. Subsequently, the mixed solution was transferred into a quartz cuvette to further NIR luminescence spectra measurement.

Temperature calibration curve of DRLNT in skin tissue mimicking phantom

The differences between emission intensity generated by the luminescent nanothermometer (I_{real}) and the intensity detected by the spectrometer (I_{exp}) could be explained by the extinction coefficient[9-10]. As indicated in recent studies, $I_{exp} = I_{real} \cdot \exp(-\alpha/l)$, where α is the extinction coefficient at the analyzed wavelength and l is the medium thickness. The tissue-mimicking phantom was composed of gelatin, intralipid and hemoglobin, which were used to control the stability, scattering coefficient (μ_s) and absorption coefficient (μ_a), respectively. The scattering and absorbing properties of phantom and skin were computed using the inverse adding-doubling method[11]. By controlling the

concentration of the components, the extinction coefficient (α)[12], which equals the sum of the extinction coefficient and the scattering coefficient of the synthetic gelatin-like phantom was compared with that of the skin both with 0.2 mm thickness, showing a good match. The relative error of the extinction coefficient value of the tissue and the skin at 1215 nm, 1330 nm and 1470 nm were 0.04, 0.06, 0.10 respectively, which meant that the gelatin model could simulate the tissue model in vivo very well.

For measurement of temperature calibration curve in tissue phantom, the entire experimental instrument configuration was identical to those in the aqueous solution, but the dispersion was substituted by tissue phantom. Schematic diagram of temperature monitoring in tissue phantom is shown in Figure S17. DRLNT@PEG dispersed in tissue phantom was tested irradiated by a CW 808 nm laser.

Bioimaging and temperature monitoring in vivo.

Mouse inflammation model: Animal procedures in this study were approved by the Institutional Animal Care and Use Committee (IACUC), ShanghaiTech University and were performed in accordance with the guidelines of the IACUC, ShanghaiTech University. The establishment of mouse model of inflammation was according to a modified literature procedure[13]. 0.7 % (w/v) carrageenan solution in saline were injected subcutaneously into the plantar hind paw to induce inflammation.

Whole-body NIR luminescence bioimaging was realized by a 0–5 W adjustable continuous wave 808 nm diode laser (Connet Fiber Optics Co., China) as excitation source. The Optical and X-ray Small Animal Imaging System (In-Vivo Xtreme, Bruker Corporation, America) was provided as the signal collector. 1200 nm band-pass and 1400 nm long-pass filters were used to acquire in vivo imaging at the wavelength of 1215 nm and 1470 nm, respectively. DRLNT@PEG (10 mg ml^{-1}, 20 μl) dispersed in 0.9 % NaCl saline was injected into the hind paw of mouse injected with carrageenan solution. NIR bioimaging was performed one hour after the injection of DRLNT@PEG.

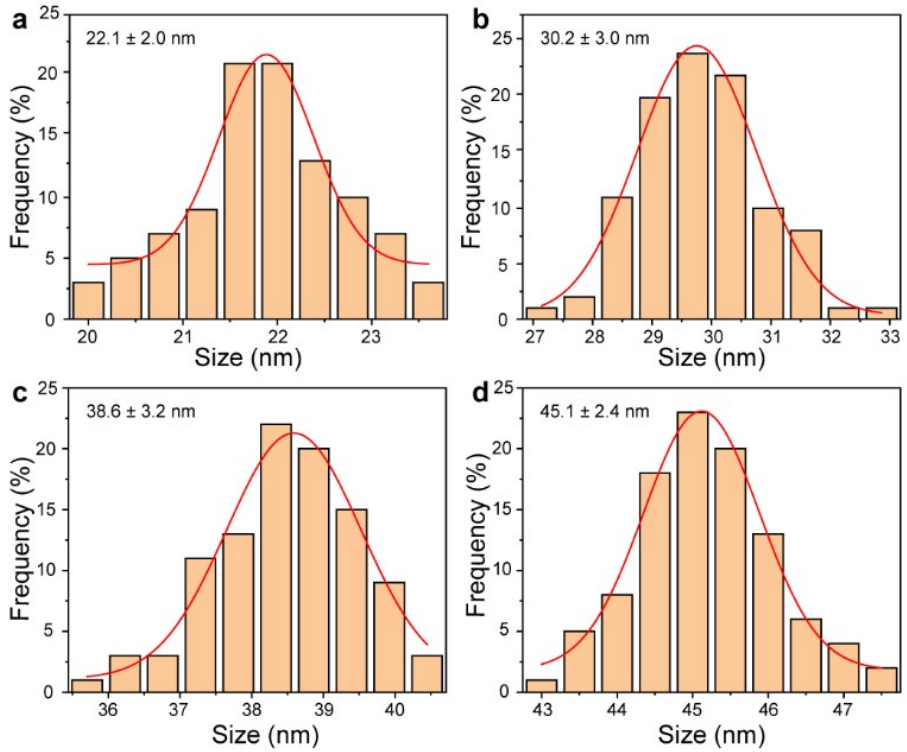

Figure S1. The size distribution of (a) $NaGdF_4$:Yb,Tm (CNP), (b) $NaGdF_4$:Yb,Tm@$NaYF_4$:Yb (CS1NP), (c) $NaGdF_4$:Yb,Tm@$NaYF_4$:Yb@$NaGdF_4$:Yb,Nd (CS2NP) and (d) $NaGdF_4$:Yb,Tm@$NaYF_4$:Yb@$NaGdF_4$:Yb,Nd@$NaGdF_4$ (DRLNT).

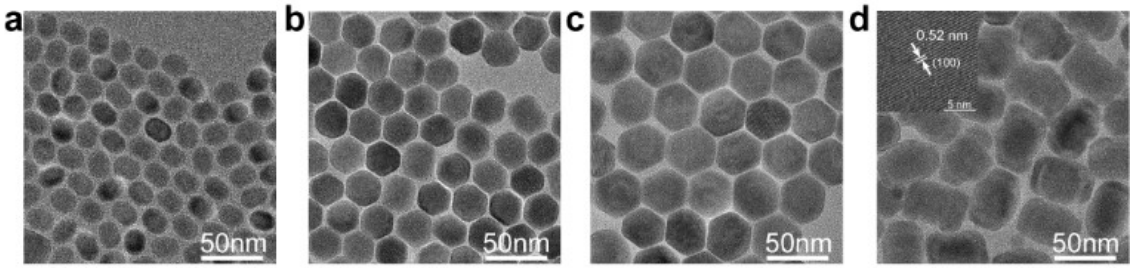

Figure S2. Transmission electron microscope (TEM) of (a) $NaYF_4$:49%Yb,1%Tm (Y-CNP), (b) $NaYF_4$:49%Yb,1%Tm@$NaYF_4$:20%Yb (Y-CS1NP), (c) $NaYF_4$:49%Yb,1%Tm@$NaYF_4$:20%Yb @$NaGdF_4$:10%Yb,25%Nd (Y-CS2NP) and (d) $NaYF_4$:49%Yb,1%Tm@$NaYF_4$:20%Yb @$NaGdF_4$:10%Yb,25%Nd@$NaYF_4$ (Y-CS3NP). The inset is the High resolution TEM image of Y-CS3NP, which indicated good crystallinity and the (1 0 0) lattice plane of hexagonal phase Y-CS3NP.

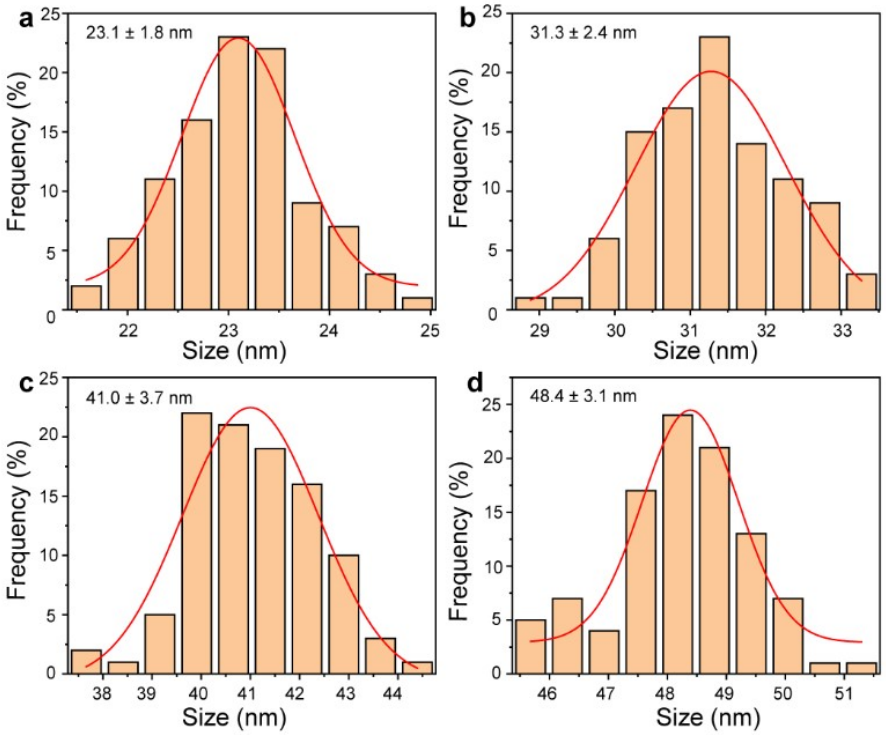

Figure S3. The particle size distribution of (a) $NaYF_4$:Yb,Tm (Y-CNP), (b) $NaYF_4$:Yb,Tm@$NaYF_4$:Yb (Y-CS1NP), (c) $NaYF_4$:Yb,Tm@$NaYF_4$:Yb@$NaYF_4$:Yb,Nd (Y-CS2NP) and (d) $NaYF_4$:Yb,Tm@$NaYF_4$:Yb@$NaYF_4$:Yb,Nd@$NaYF_4$ (Y-CS3NP).

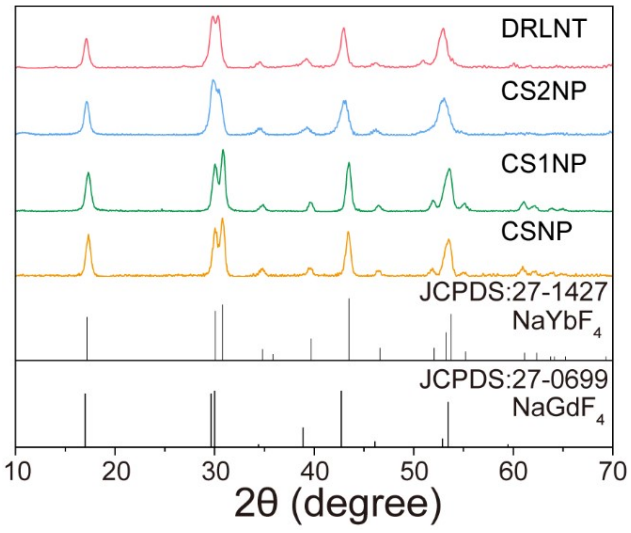

Figure S4. X-ray powder diffraction (XRD) analysis of DRLNT and its intermediates.

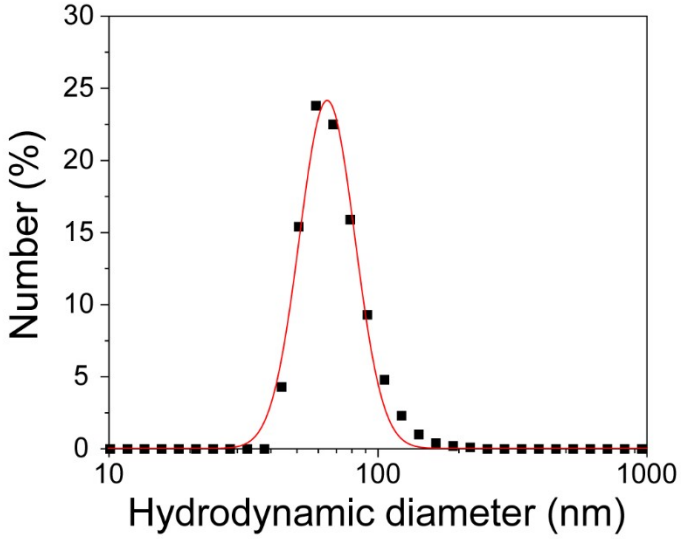

Figure S5. Dynamic light scattering (DLS) analysis of DRLNT@PEG dispersed in deionized water and a log-normal function fit to obtain the size distribution. The hydrodynamic size was calculated to be 68.5 nm and the corresponding error was 0.24.

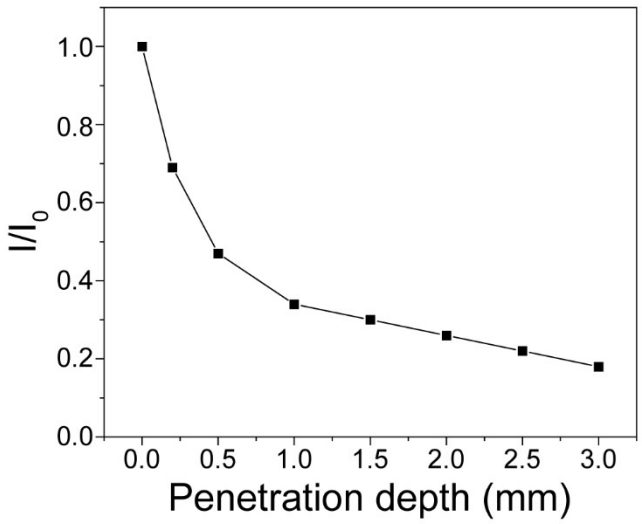

Figure S6. Decay of NIR emission intensity of DRLNT with different depths of tissue.

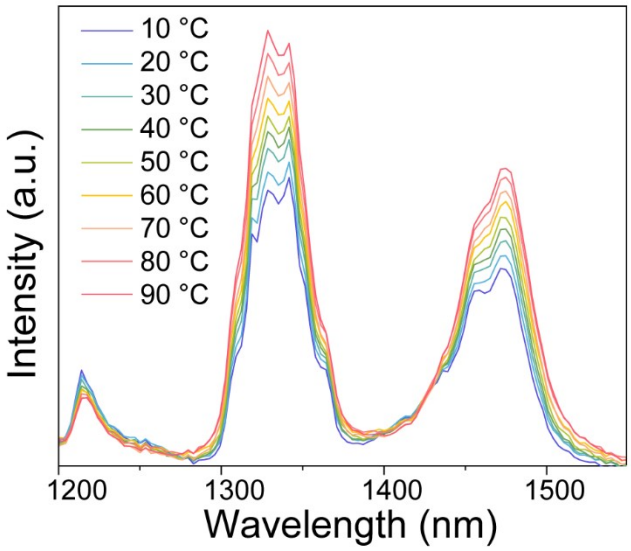

Figure S7. The absolute intensity changes for NIR luminescence spectra of DRLNT@PEG in aqueous solutions at 10 to 90 °C by external heating.

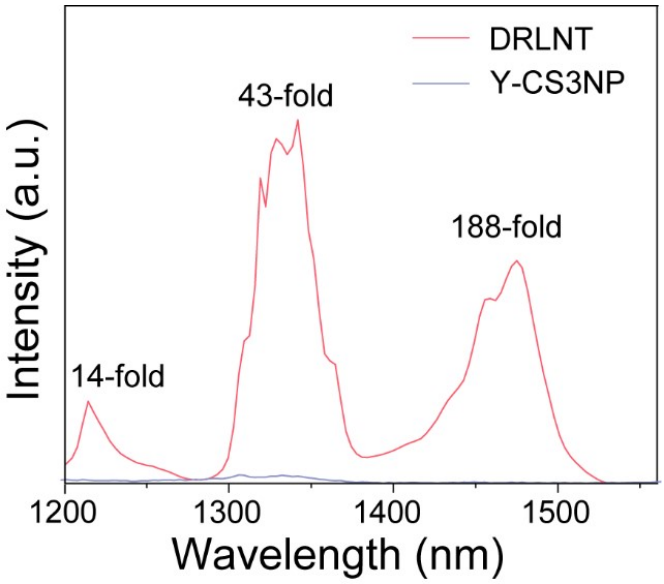

Figure S8. Near infrared (NIR) luminescence spectra of DRLNT and Y-CS3NP in aqueous solutions. The concentrations of Tm^{3+} ions and the experiment environment were kept the same.

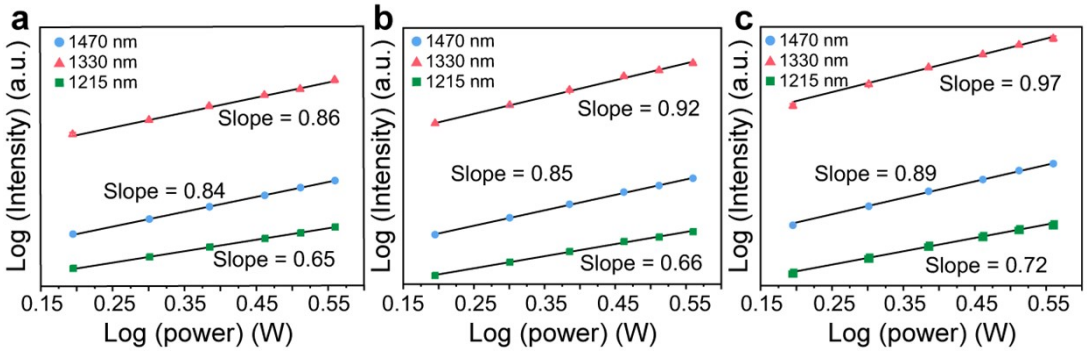

Figure S9. Plots of logarithmic excitation power *versus* logarithmic emission intensities of DRLNT at 1215 nm, 1330 nm and 1470 nm, respectively, in aqueous solutions excited by 808 nm. The plots were collected at (a) 30 °C, (b) 50 °C and (c) 70 °C, respectively.

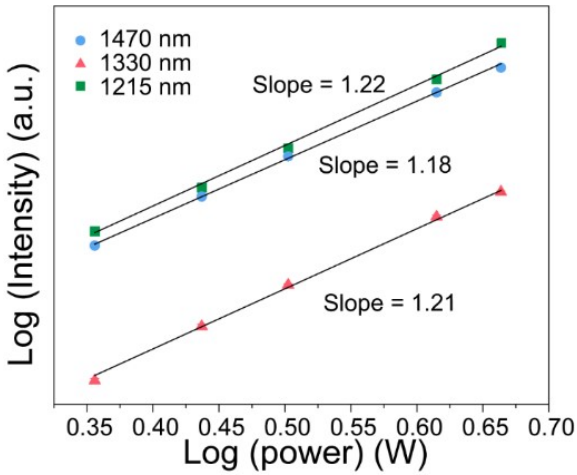

Figure S10. Plots of logarithmic excitation power *versus* logarithmic emission intensities of DRLNT at 1215 nm, 1330 nm and 1470 nm, respectively, in aqueous solutions excited by 980 nm laser. The plots were collected at 30 °C.

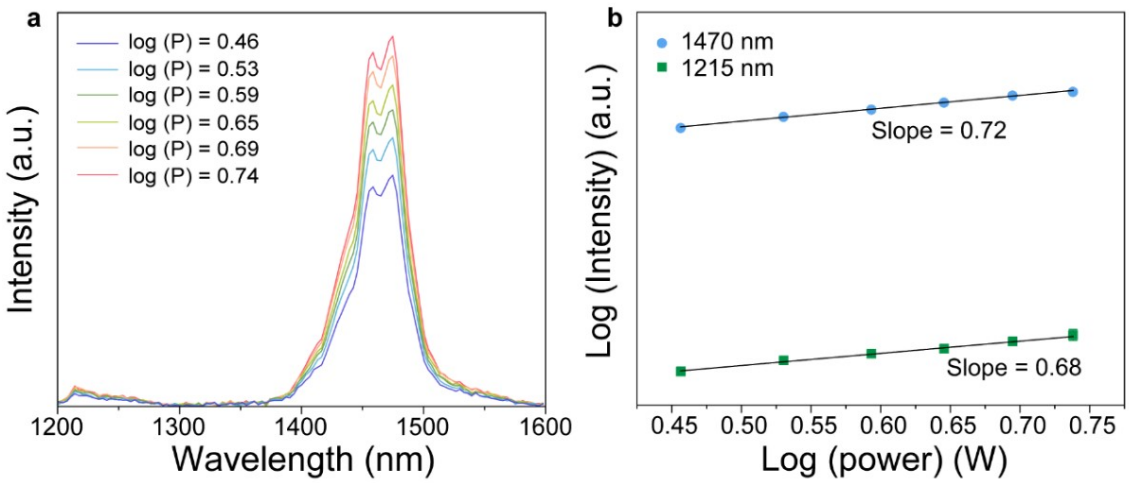

Figure S11. (a) NIR luminescence spectra of $NaGdF_4$:Yb,Tm@$NaYF_4$:Yb@$NaGdF_4$:Yb@$NaGdF_4$ nanoparticles without Nd^{3+} doping under 808 nm excitation with different powers. Nanoparticles were dispersed in aqueous solutions at 30 °C. (b) Plots of logarithmic excitation power *versus* logarithmic emission intensities of $NaGdF_4$:Yb,Tm@$NaYF_4$:Yb@$NaGdF_4$:Yb@$NaGdF_4$ at 1470 nm in aqueous solutions excited by 808 nm laser.

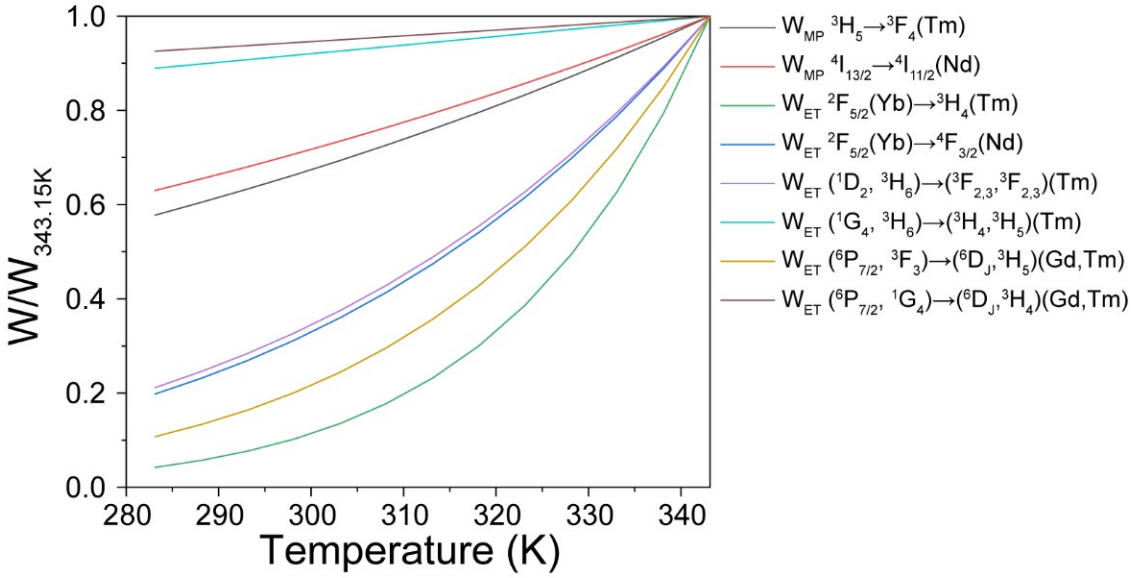

Figure S12. Nonradiative decay rates due to energy transfer and multiphonon relaxation upon temperature in $NaGdF_4$ matrix. The plots were normalized at 343.15 K.

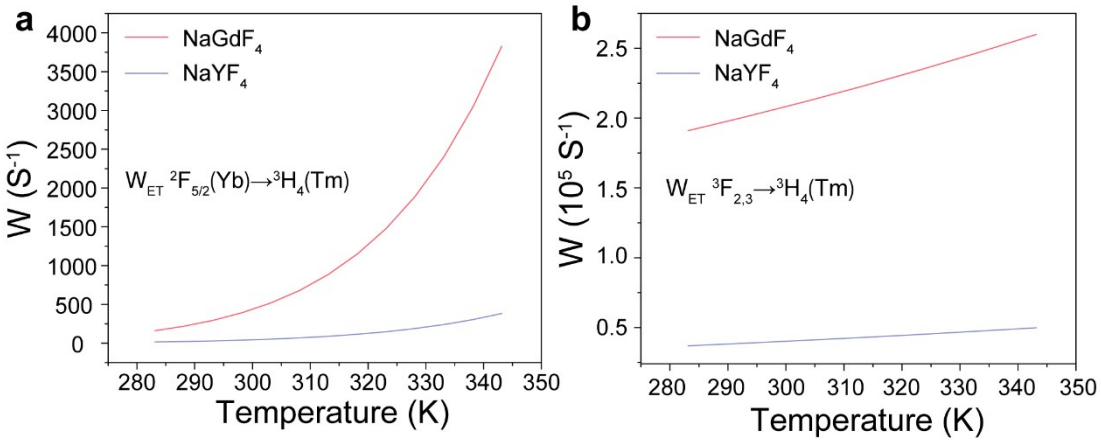

Figure S13. (a) The energy transfer rate of $^2F_{5/2}$ (Yb^{3+})→$^3H_4$ (Tm^{3+}) and (b) the multiphonon relaxation rate $^3F_{2,3}$→$^3H_4$ (Tm^{3+}) upon temperature in $NaGdF_4$ and $NaYF_4$ matrix.

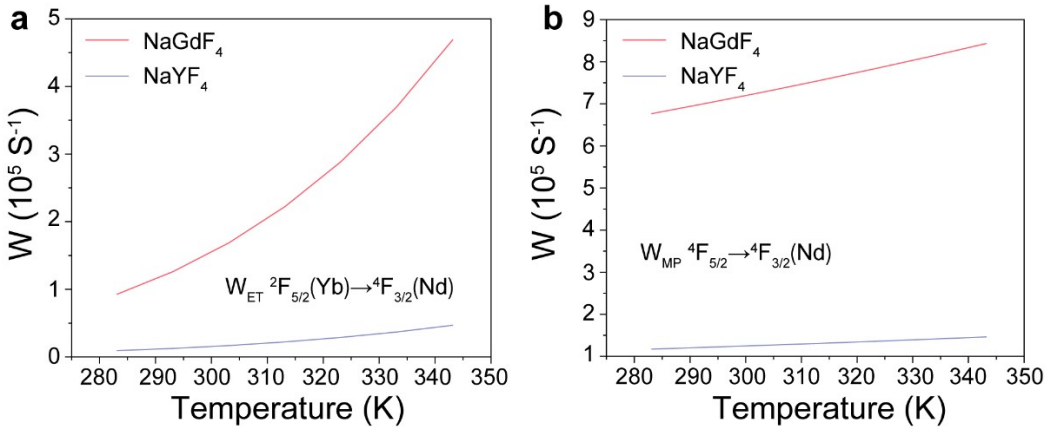

Figure S14. (a) The energy transfer rate $^2F_{5/2}$ (Yb^{3+})→$^4F_{3/2}$ (Nd^{3+}) and (b) the multiphonon relaxation rate $^4F_{5/2}$→$^4F_{3/2}$ (Nd^{3+}) upon temperature in $NaGdF_4$ and $NaYF_4$ matrix.

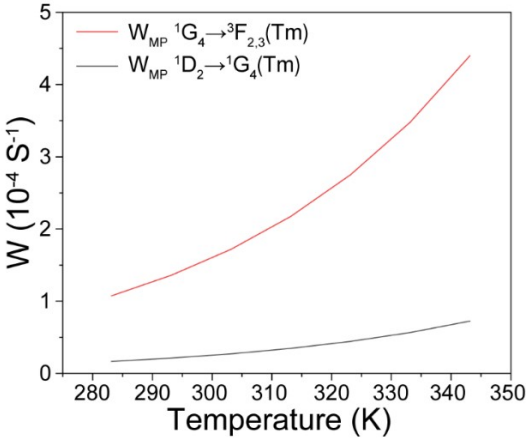

Figure S15. Multiphonon relaxation rate of $^1D_2$ ($^1D_2$→$^1G_4$) and $^1G_4$ ($^1G_4$→$^3F_{2,3}$) upon temperature

in $NaGdF_4$ matrix.

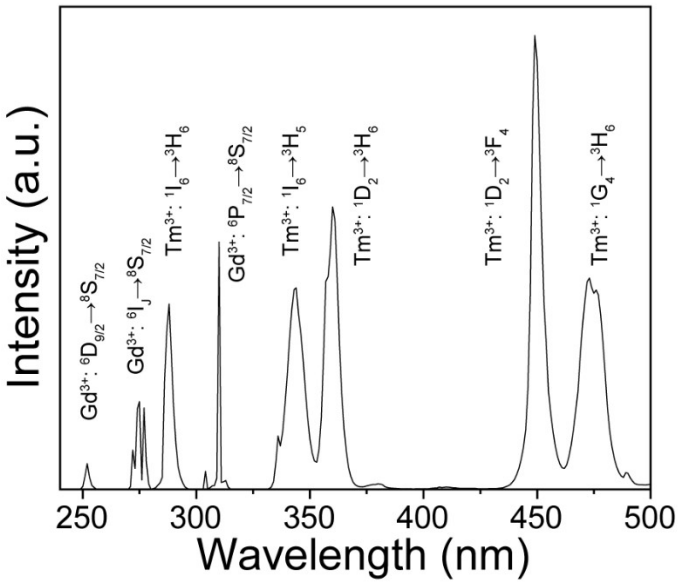

Figure S16. Room-temperature ultraviolet to visible emission spectra of DRLNT nanocomposite under 808 nm excitation.

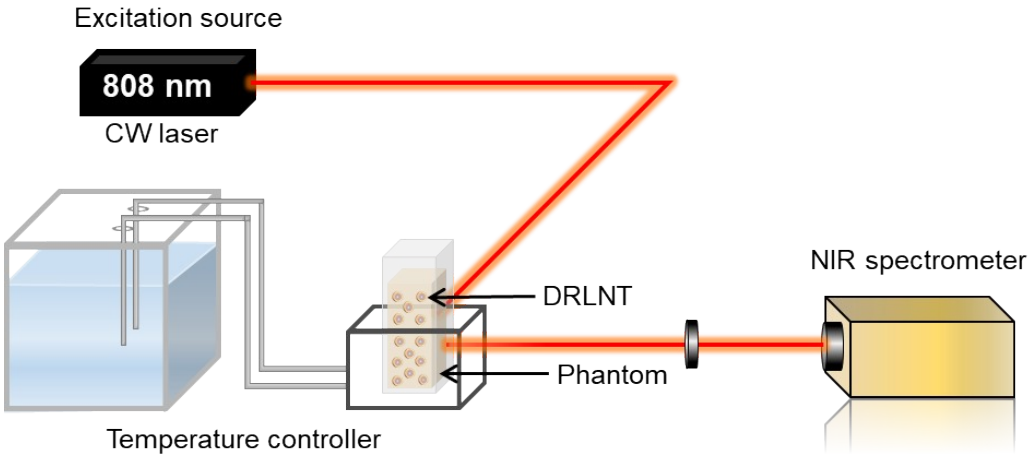

Figure S17. Schematic diagram of the detection of the temperature response of DRLNT in phantom.

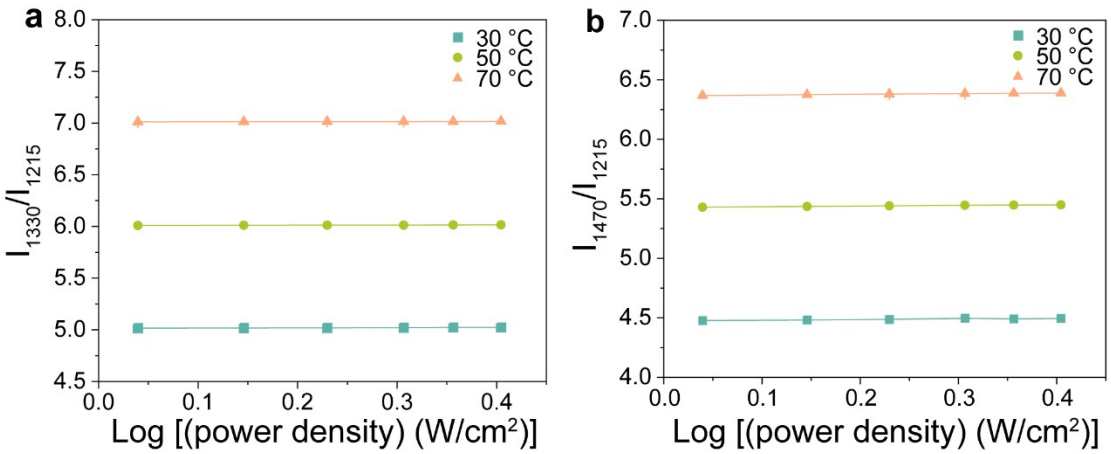

Figure S18. Emission ratios of I_{1330}/I_{1215} and I_{1470}/I_{1215} corresponding to probe-Nd (a) and probe-Tm (b) in DRLNT under different excitation power density.

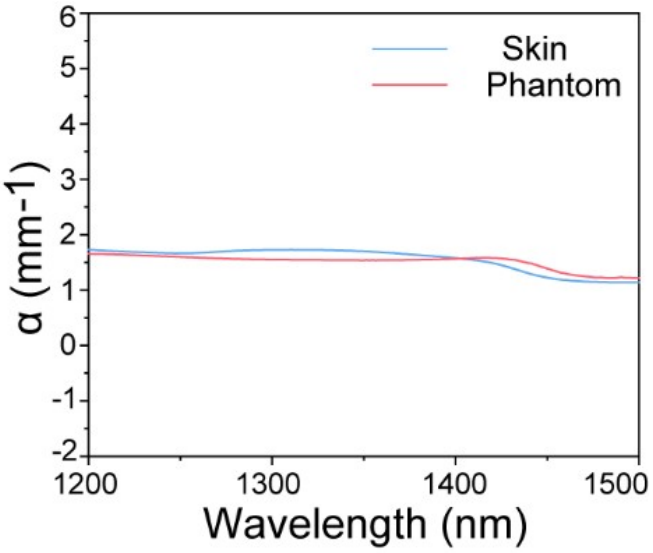

Figure S19. The extinction coefficient of tissue mimicking phantom and the skin of mouse paw.

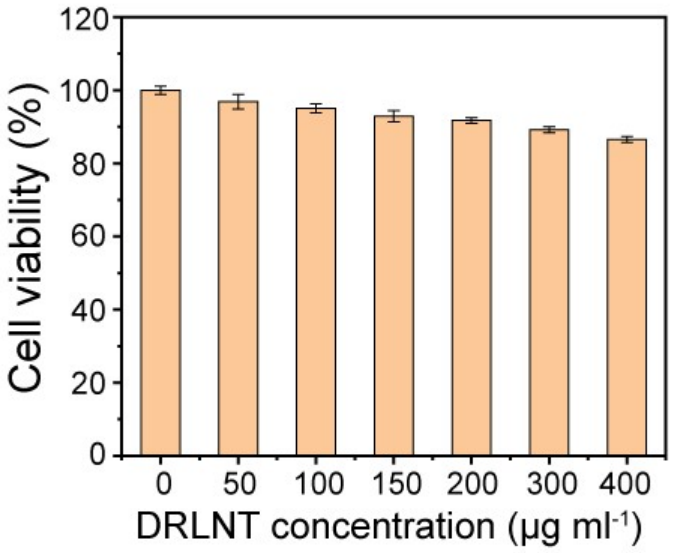

Figure S20. Methyl thiazolyl tetrazolium (MTT) assays of DRLNT@PEG in HEK 293T cells. Error bars were defined as s.d. ($n = 3$).

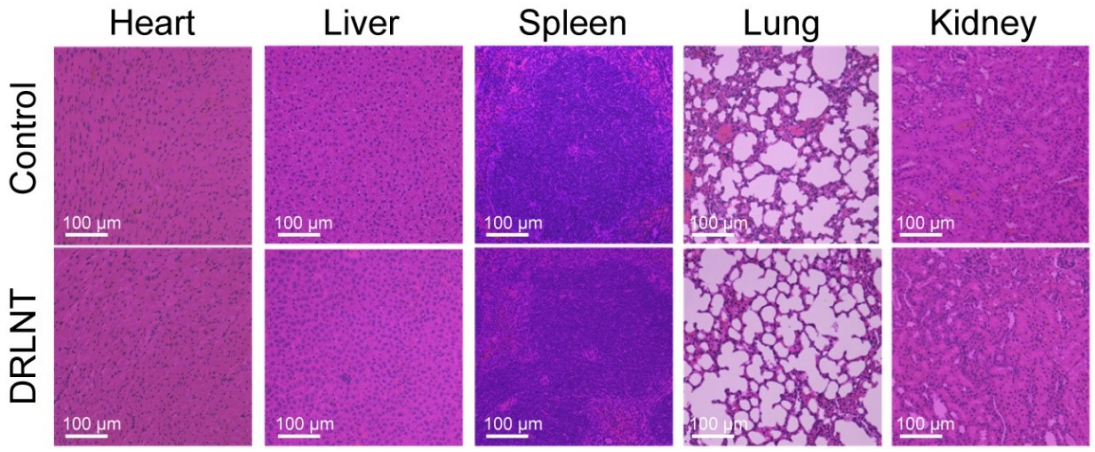

Figure S21. Hematoxylin and eosin (H&E)-stained tissue sections (heart, liver, spleen, lung, kidney) from control mouse without injection of DRLNT@PEG and mouse injected with DRLNT@PEG.

Table S1. The quantum yield (%) of DRLNT and Y-CS3NP samples for NIR emissions.

Emission Wavelength (nm) / Sample	1215	1330	1470
DRLNT	0.25	1.87	1.52
Y-CS3NP	0.013	0.63	0.061

Table S2. Uncertainty of probe Tm and probe Nd in tissue phantom at 10 to 70 °C.

Temperature (°C) / Probe	10	20	30	40	50	60	70
Tm	0.33	0.63	0.30	0.35	0.35	0.50	0.38
Nd	0.29	0.40	0.31	0.41	0.34	0.62	0.45

References

1. E. C. Ximendes, U. Rocha, T. O. Sales, N. Fernández, F. Sanz-Rodríguez, I. R. Martín, C. Jacinto, D. Jaque, *Adv. Funct. Mater.* 2017, **27**, 1702249.
2. L. A. Riseberg, H. W. Moos, *Phys. Rev. Lett.* 1967, **19**, 1423.
3. K. Lu, Y. Yi, L. Xu, X. Sun, L. Liu, H. Li, *Nanomaterials (Basel)* 2019, **10**, 24.
4. L. Xu, H. Zheng, T. Pang, J. Mao, *J. Rare Earths* 2022, **40**, 406.
5. F. Auzel, *Phys. Rev. B* 1976, **13**, 2809.
6. L. Labrador-Paez, M. Pedroni, A. Speghini, J. Garcia-Sole, P. Haro-Gonzalez, D. Jaque, *Nanoscale* 2018, **10**, 22319.
7. M. Jia, Z. Sun, H. Xu, X. Jin, Z. Lv, T. Sheng, Z. Fu, *J. Mater. Chem. C* 2020, **8**, 15603.
8. A. M. Degrand, S. J. Lomnes, D. S. Lee, M. Pietrzykowski, S. Ohnishi, T. Morgan, A. Gogbashian, R. G. Laurence and J. V. Frangioni, *J. Biomed. Opt.*, 2006, **11**, 014007.
9. A. Bednarkiewicz, L. Marciniak, L. D. Carlos, D. Jaque, *Nanoscale* 2020, **12**, 14405.
10. B. del Rosal, E. Ximendes, U. Rocha and D. Jaque, *Adv. Opt. Mater.*, 2017, **5**, 1600508.
11. S. A. Prahl, M. J. C. van Gemert, and A. J. Welch, *Appl. Opt.*, 1993, **32**, 559.
12. T. L. Troy, S. N. Thennadil, *J. Biomed. Opt.*, 2001, **6**, 167.
13. K. E. McCarson, *Curr. Protoc. Pharmacol.*, 2012, **56**, UNIT 5.4.